Physical Models and Application
https://www.sciltp.com/journals/pma

Article

Physical Modeling and Firing Patterns Analysis of a Josephson Junction-Based Ion Channel Neuron

Kailong Zhu and Feifei Yang *

College of Artificial Intelligence and Computer Science, Xi'an University of Science and Technology, Xi'an 710054, China
* Correspondence: dlpuyff@sina.com

How To Cite: Zhu, K.; Yang, F. Physical Modeling and Firing Patterns Analysis of a Josephson Junction-Based Ion Channel Neuron. *Physical Models and Application* **2026**, *1*(1), 2.

Received: 15 August 2026
Revised: 4 September 2026
Accepted: 30 September 2026
Published: 15 October 2026

Abstract: The electrical activity of biological neuron stems from the time-varying coupling of electromagnetic fields inside and outside the cell membrane, and the directional migration of ions across the membrane. Therefore, a physically motivated circuit-level emulation of nonlinear ion-channel currents can facilitate the analysis of selected electrical activity features of neurons. This work presents a Josephson Junctions (*JJ)* based ion channel neuron model at the circuit level, where a *JJ* branch is employed to emulate the nonlinear conductance of an effective ion-channel branch in the neuronal equivalent circuit. The capacitance characteristics of the cell membrane are simulated using capacitors. The nonlinear dynamic model of the neuron is developed by applying Kirchhoff's laws. Through dynamic analysis and numerical simulation of the model, the firing patterns of this neuron under different external stimuli and external magnetic fields are studied. The results show that this model could reproduce selected periodic and chaotic firing-like dynamical patterns. Moreover, the model is further examined using analog circuit emulation and DSP implementation. Therefore, the ion channel neuron model based on *JJ* can emulate selected nonlinear ion-channel-current effects and firing dynamics at a phenomenological circuit level, providing a new circuit-level modeling approach for neuromorphic hardware design.

Keywords: neuron model; Josephson Junctions ion channel; firing behaviors; hardware implementation

1. Introduction

The biological neuron model is essentially a mathematical description of the properties of neurons, aiming to accurately describe and predict biological processes. Accurate neuron models play a crucial role in revealing the functions, communication, and disease mechanisms of neurons, helping to deepen our understanding of the complexity of the brain, cognition, and consciousness. Neuron models are also widely applied in the research of neurological diseases. At first, some biological neuron models have been obtained through both biological experiments and mathematical theories, for instance Hodgkin–Huxley (HH) neuron [1], FitzHugh–Nagumo (FHN) neuron [2,3], Morris–Lecar (ML) neuron [4], Hindmarsh–Rose (HR) neuron [5], Chay neuron [6], Izhikevich spiking neuron [7] and Chialvo map neuron [8]. These models differ in state dimension and biological detail (HH: four variables; FHN, ML, and Izhikevich: two variables; HR: three variables). The present two-variable circuit model uses the *JJ* branch to emulate effective nonlinear ion-channel conductance rather than detailed ionic gating.

Based on these existing models of biological neurons, some improved neuron models have been proposed, for example, the memristive FHN neuron [9,10], memristive HR neuron [11–13] and memristive Chialvo map neuron [14], memristive ML neuron [15], memristive Rulkov neuron map [16]. These neuron models are obtained by introducing a memristor into the existing neuron models. Recently, some biological neuron models have been established through physical circuits, such as memristive membrane neuron [17–19], memristive ion channel

Copyright: © 2026 by the authors. This is an open access article under the terms and conditions of the Creative Commons Attribution (CC BY) license (https://creativecommons.org/licenses/by/4.0/).
Publisher's Note: Scilight stays neutral with regard to jurisdictional claims in published maps and institutional affiliations.

neuron [20–22], Josephson Junction neuron [23–25], map neuron [26–28]. In particular, Ref. [23] employs two capacitors linked by a linear resistor and a *JJ* for magnetic-field effects, whereas the present circuit contains one capacitor, a nonlinear resistor, and a *JJ* branch. The former emphasizes double-capacitive energy dynamics, while the present model focuses on firing patterns in a single-capacitor circuit. These neuron models are implemented via distinct nonlinear circuits assembled from a range of electronic components. A detailed description of the modeling method for neuron model that are based on physical circuit can be found in the Refs [29,30].

Furthermore, some coupled neural systems have also been studied, for example, coupled FHN neuron system [31], coupled neuron network [32]. In coupled neuron system, various characteristics have been analyzed, such as the synchronization characteristics [33–35], energy balance [36,37], heterogeneity [38], defects [39], pattern formation [40–42], associative memory characteristic [43], synchronization control feature [44] and stability of synchronization [45–47]. Further details on the feature of neuron and the memristive neuron network can be found in Refs. [48,49] and [50], respectively. Furthermore, Recent work has shown that chaotic background spike trains can modulate weak-signal processing in a Hodgkin–Huxley neuron [51], highlighting the relevance of characterizing chaotic firing in physical neuron models.

In recent years, *JJ* have been widely regarded as potential candidate devices for constructing novel neuromorphic computing units due to their inherent nonlinear current-voltage characteristics, natural relaxation oscillation behavior. This paper presents a *JJ*-based ion channel neuron model at the circuit level. The Josephson junction is used to emulate the nonlinear conductance of an effective ion-channel branch, rather than to reproduce a particular biological ion channel, and capacitors are employed to represent the charging and discharging behavior of the cell membrane's capacitance. The mathematical description of this equivalent circuit is established using Kirchhoff's laws, and nonlinear dynamic equations are derived. On this basis, this paper systematically studies the discharge patterns of the model under different external excitation currents and external magnetic fields. Through numerical simulation and dynamic analysis, periodic discharges and chaotic behaviors within the parameter space are revealed. Further, to verify the practical feasibility of the model, the analog circuit emulation and DSP implementation is carried out separately.

2. Physical Modeling of Neuron

The physical neurons modeled based on the equivalent circuits of capacitors, resistors, voltage sources, and nonlinear electronic components have multiple theoretical and engineering values. Therefore, this paper designs a neuron equivalent circuit of capacitor (*C*), resistor (*Rs*), voltage source (*Vs*), *JJ* and nonlinear resistor (R_N). Here, Figure 1 provides a circuit structure diagram.

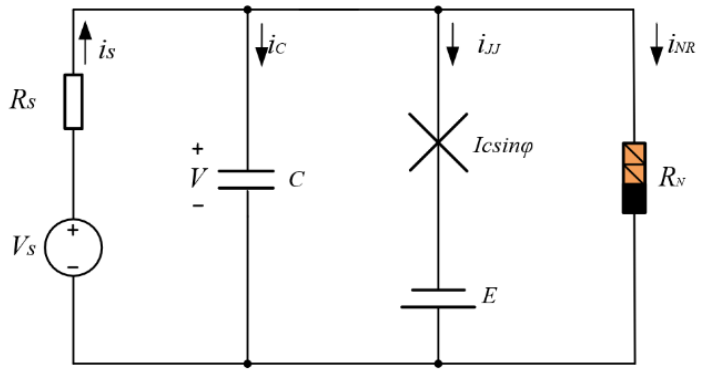


Figure 1. A circuit structure diagram.

The current characteristics of the *JJ* can be approached by

$$i_{JJ} = I_c \sin(\varphi); \frac{d\varphi}{dt} = \frac{2e}{\hbar} V_{JJ}, \tag{1}$$

where I_c is the critical current, φ denotes phase difference, e means the elementary charge and $\hbar$ is the reduced Planck constant. The current in the R_N branch can be approached by

$$i_N = -\frac{1}{\rho}(V - \frac{V^3}{3V_0^2}), \tag{2}$$

where ρ and V_0 are the characteristic resistance and cutoff voltage of R_N, respectively. The current can be obtained as follows

$$i_s = \frac{V_S - V}{R_S}, \tag{3}$$

where V_s is the external input voltage and R_s is the resistor connected to the voltage source.

According to Kirchhoff's circuit laws, the equations of the neural circuit in Figure 1 can be presented by

$$\begin{cases} C\dfrac{dV}{dt} = \dfrac{V_S - V}{R_s} - I_c \sin(\varphi) + \dfrac{1}{\rho}(V - \dfrac{V^3}{3V_0^2}); \\ \dfrac{d\varphi}{dt} = \dfrac{2e}{\hbar}(V + E). \end{cases} \tag{4}$$

To obtain a dimensionless dynamic model, the variables and parameters in Equation (4) are redefined as

$$x = \frac{V}{V_0}, z = \varphi, \tau = \frac{t}{\rho C}, u_s = \frac{V_s \rho}{R_s V_0}; a = \frac{\rho}{R_s}, \beta = \frac{I_c \rho}{V_0}, \mu = \frac{2eV_0 \rho C}{\hbar}, \eta = \frac{E}{V_0}. \tag{5}$$

where x is the normalized circuit voltage, z is the Josephson phase difference, and u_s is the normalized external voltage.

The parameters a, β, μ, and η represent the resistance ratio, normalized *JJ* critical-current strength, time-scale factor, and normalized effective phase-driving voltage, respectively. In Equation (4), V, V_s, V_0, and E are in V; C, R_s, ρ, I_c, and t are in F, Ω, Ω, A, and s, respectively. Therefore, x, z, τ, u_s, a, β, μ, and η are dimensionless. Substitution of Equation (5) into Equation (4) gives Equation (6). A dimensionless dynamic model can be presented by

$$\begin{cases} \dfrac{dx}{d\tau} = (1-a)x - \dfrac{1}{3}x^3 - \beta \sin(z) + u_s; \\ \dfrac{dz}{d\tau} = \mu(x + \eta); \end{cases} \tag{6}$$

The *JJ* branch emulates effective ion-channel conductance through $\beta\sin(z)$, while z is not a biological gating variable. Thus, the model does not represent ionic selectivity or detailed sodium/potassium activation–inactivation kinetics. In the following analysis, the periodic voltage signal is selected as $u_s = A\cos(ft)$, A and f represent the amplitude and frequency of the external stimulus, respectively. Sinusoidal stimulation is selected because its amplitude and frequency can be independently varied, allowing the effects of periodic driving on the model dynamics to be examined systematically. Pulse-driven firing will be considered in future work.

Since Josephson junctions are sensitive to magnetic fields through field-induced changes in phase and critical current. Accordingly, the dynamic model in Equation (6) is represented by

$$\begin{cases} \dfrac{dx}{d\tau} = (1-a)x - \dfrac{1}{3}x^3 - \beta \sin(z) + u_s; \\ \dfrac{dz}{d\tau} = \mu(x + \eta) + S_{ext}; \end{cases} \tag{7}$$

where S_{ext} is an effective normalized signal representing magnetic-field-induced modulation; its constant and periodic forms represent constant and periodic magnetic excitation, respectively.

3. Firing Patterns Analysis

Firing patterns of neuron are analyzed in this section. At first, parameters in Equation (6) are fixed as a = 0.25, β = 0.8, μ = 0.2, η = 0.9. In addition, initial value in Equation (6) are given as (0.1, 0.1). In the MATLAB software, bifurcation diagrams were computed using ode23 (RelTol = 10^{-8}, AbsTol = 10^{-10}, and MaxStep = 0.05). LLEs were obtained using ode45 with the variational equations and the Gram–Schmidt method (RelTol = 10^{-9}, AbsTol = 10^{-11}, and interval 0.01); the first 600 time units were discarded from a 1200-unit integration. Convergence was accepted when the latest 101 estimates varied by less than 10^{-3} after 1000 post-transient intervals.

For the case of $u_s = A\cos(0.34\tau)$, the bifurcation diagram obtained from the local extrema of x and the corresponding largest Lyapunov exponent (*LLE*) are shown in Figure 2 as A varies. Chaos was identified by a positive converged *LLE*, supported by the bifurcation structure and representative firing sequences; near-zero *LLE* values were treated as indeterminate rather than chaotic. Under periodic driving, firing depends on A, f, and system

parameters; thus, no unique parameter-independent threshold is defined. The transitions are characterized by the bifurcation diagrams and *LLE* curves.

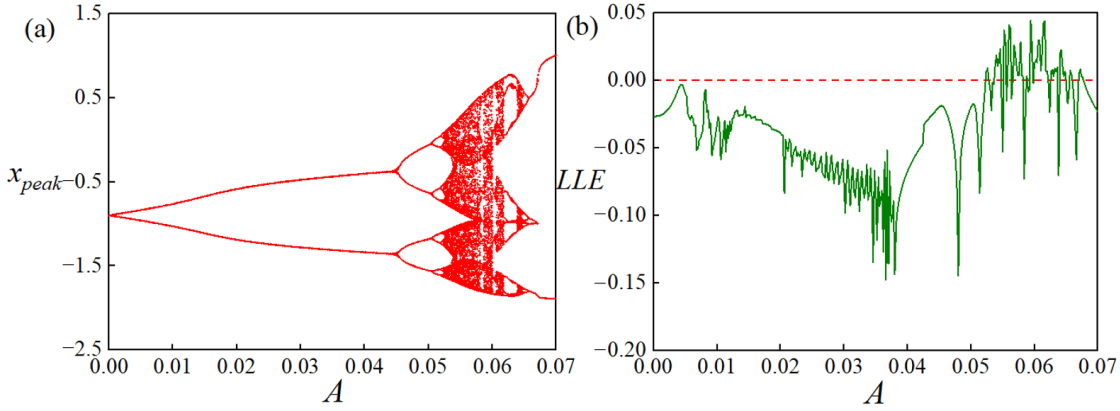


Figure 2. Firing behavior of neuron for varying values of *A*. For (**a**) Evolution of bifurcation diagram; (**b**) *LLE* curve.

From Figure 2, the various of periodic firing behaviors and chaotic firing patterns can be triggered by applying different amplitudes of periodic external stimulation. Furthermore, the typical firing sequences corresponding to the different amplitudes of periodic external stimuli are plotted in Figure 3.

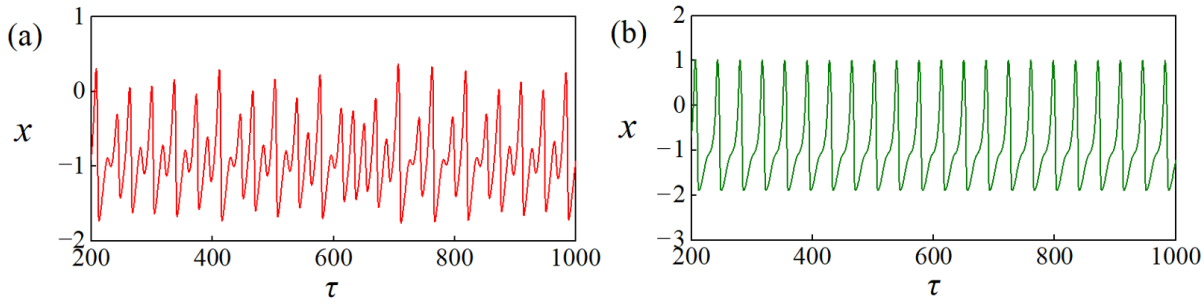


Figure 3. The firing sequences corresponding to different amplitudes *A*. For (**a**) $A = 0.055$; (**b**) $A = 0.07$.

Figure 3 shows that the chaotic firing behavior exhibits disorder and non-periodicity, while the periodic firing behavior has a high degree of orderliness. Similarly, for the case of $u_s = 0.055\cos(f\tau)$, bifurcation diagram by changing the values of *f* and its corresponding the *LLE* are Figure 4.

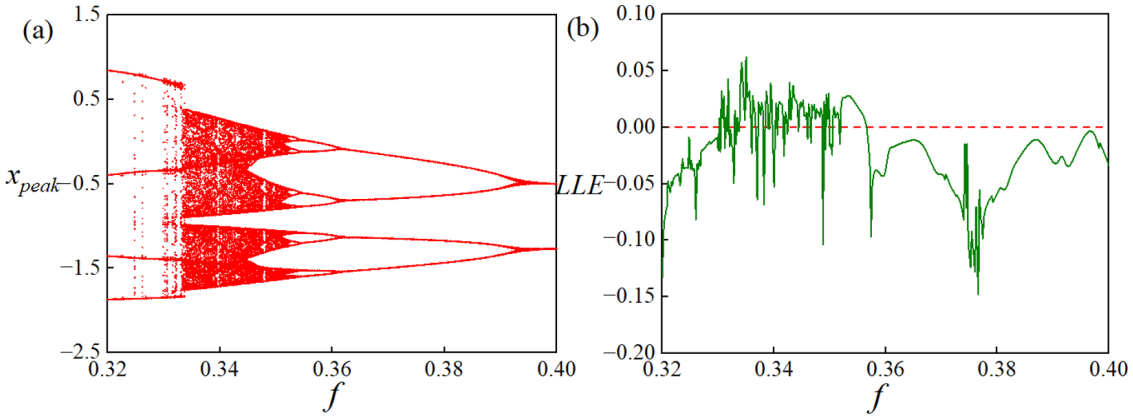


Figure 4. Firing behavior of neuron for varying values of *f*. For (**a**) Evolution of bifurcation diagram; (**b**) *LLE* curve.

Figure 4 reveals that chaotic and periodic firing patterns are obtainable under varying frequency intensities. As the frequency intensity continuously increases, the chaotic firing behavior is suppressed, thereby triggering a

periodic firing mode. Furthermore, the firing sequences under different periodic external stimulation frequencies are plotted in Figure 5.

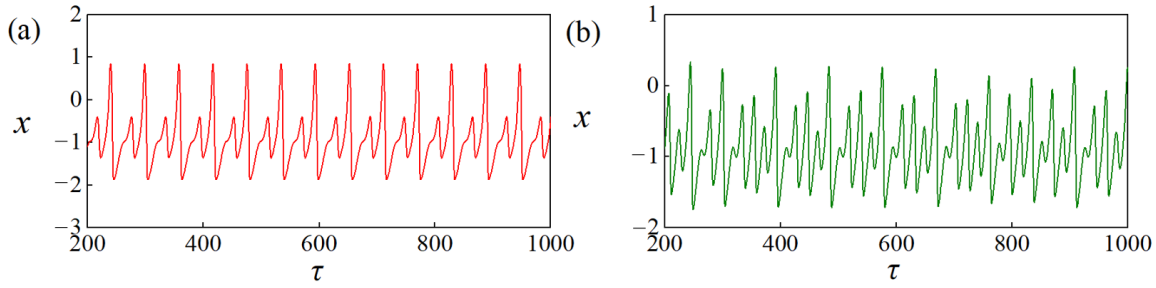


Figure 5. The firing sequences corresponding to different frequencies *f*. For (**a**) $f = 0.32$; (**b**) $f = 0.341$.

It can be clearly observed from Figure 5 that the periodic and chaotic firing behaviors induced by external periodic stimuli at different frequency intensities. In fact, the amplitude and frequency of periodic external stimuli can simultaneously change and affect the electrical activity characteristics of neurons. Therefore, by using the *SE* complexity, this paper further explores the characteristics of neuronal electrical activity when the amplitude and frequency of the external periodic simultaneously changed. The result is shown in Figure 6. Here, SE complexity is calculated from the power spectrum and used to characterize the spectral complexity of the firing sequence.

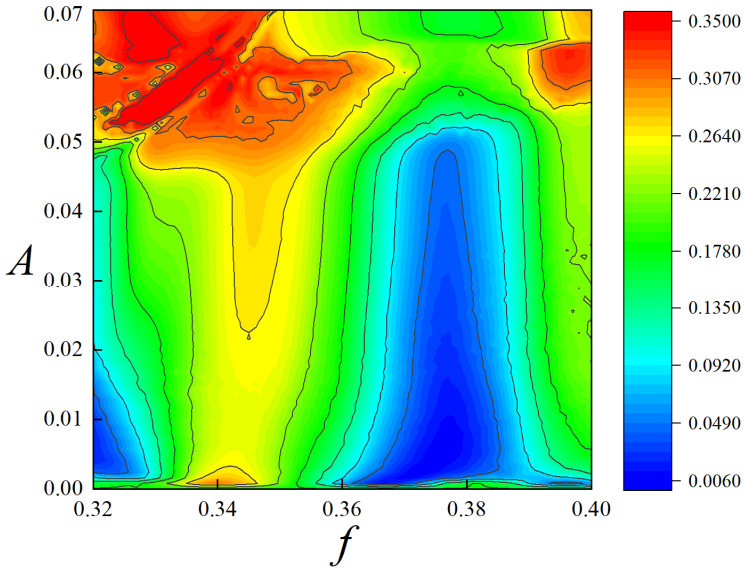


Figure 6. SE complexity. Parameters are $a = 0.25$, $\beta = 0.8$, $\mu = 0.2$, $\eta = 0.9$. Initial value is (0.1, 0.1).

From Figure 6, higher SE complexity values indicate a broader spectral distribution and more complex firing activity. The color scale is used only to display relative SE complexity and does not distinguish chaos from periodic activity. Chaos is identified from positive converged LLE values together with representative firing sequences.

The biological neuron expressed by Equation (6), is considered a nonlinear system, its dynamic characteristics can be influenced by the system parameters. Therefore, investigating the regulatory characteristics of the system parameters on the electrical activity of neurons is an interesting research topic. At first, parameters in Equation (6) are fixed as $\beta = 0.8$, $\mu = 0.2$, $\eta = 0.9$. In addition, initial value in Equation (6) is given as (0.1, 0.1), the external periodic stimuli is $u_s = 0.055\cos(0.34\tau)$. Bifurcation diagram by changing the values of a and its corresponding the *LLE* are displayed in Figure 7.

Figure 7 shows that as the parameter a increases, the periodic firing behavior can be induced to exhibit chaotic electrical activity characteristics. With the continuous increase of parameter a, the chaotic electrical activity characteristics eventually evolve into periodic discharge behavior. Furthermore, the firing sequences under values of parameter a are Figure 8.

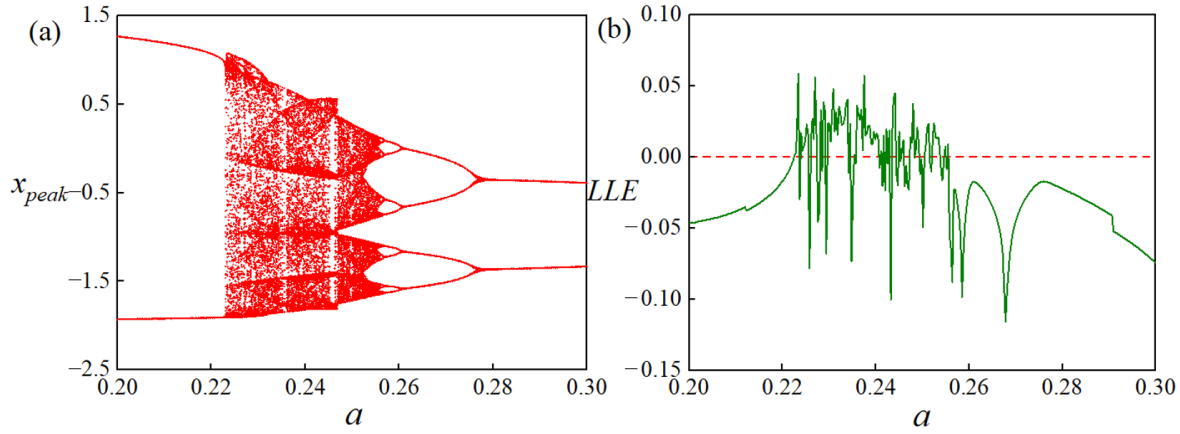


Figure 7. Firing behavior of neuron for varying values of a. For (**a**) Evolution of bifurcation diagram; (**b**) *LLE* curve.

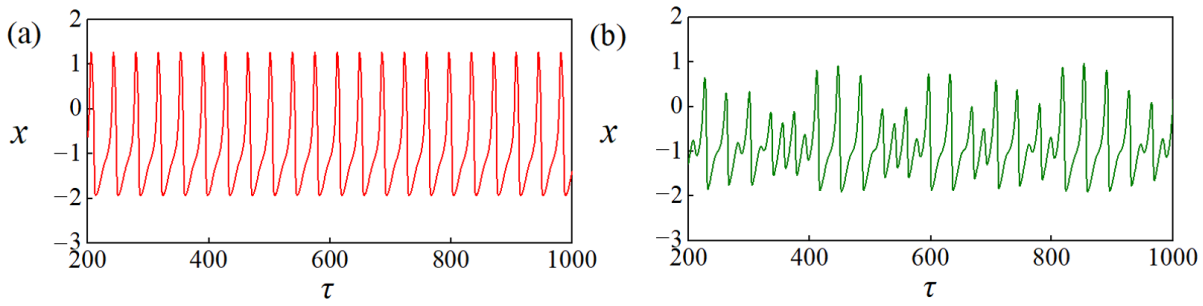


Figure 8. The firing sequences corresponding to value of a. For (**a**) $a = 0.2$; (**b**) $a = 0.23$.

It can be clearly observed from Figure 8 that the periodic and chaotic firing behaviors induced by parameter a at different values. When parameters in Equation (6) are fixed as $a = 0.25$, $\mu = 0.2$, $\eta = 0.9$, initial value in Equation (6) and the external periodic stimuli are kept as above, bifurcation diagram by changing the values of β and its corresponding the *LLE* are displayed in Figure 9.

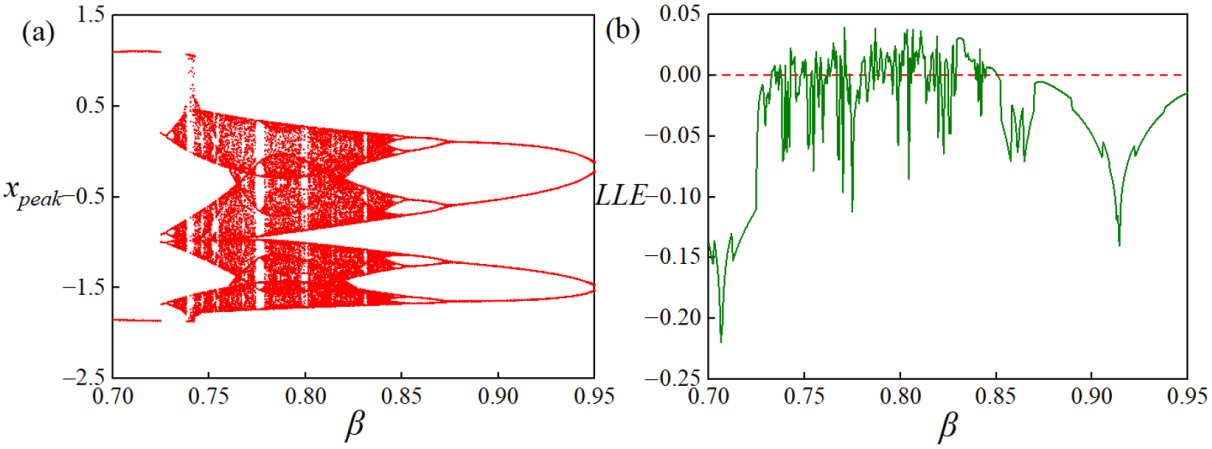


Figure 9. Firing behavior of neuron for varying β. For (**a**) Evolution of bifurcation diagram; (**b**) *LLE* curve.

Similarly, as the parameter β increases, the periodic firing behavior can be induced to exhibit chaotic electrical activity characteristics. With the continuous increase of parameter β, the chaotic electrical activity characteristics eventually evolve into periodic discharge behavior. Furthermore, the firing sequences under values of parameter β are Figure 10.

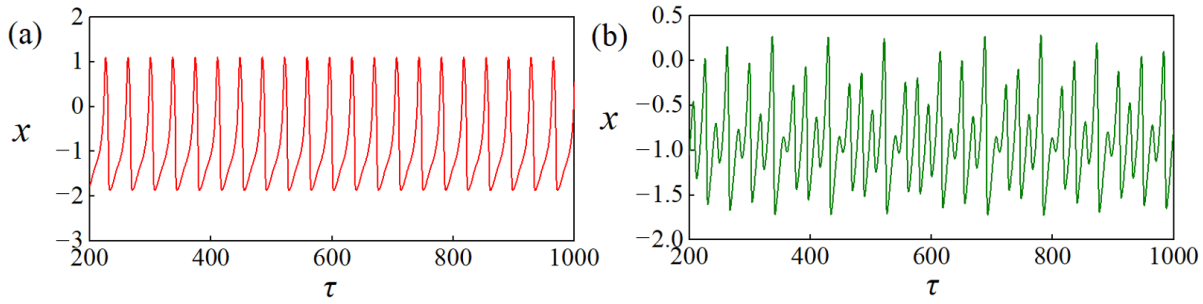


Figure 10. The firing sequences corresponding to value of β. For (**a**) $\beta = 0.71$; (**b**) $\beta = 0.81$.

Figure 10 shows that the chaotic firing behavior exhibits disorder and non-periodicity, while the periodic firing behavior has a high degree of orderliness. Similarly, parameters in Equation (6) are $a = 0.25$, $\beta = 0.8$, $\eta = 0.9$, initial values and the external periodic stimuli is kept as above, bifurcation diagram by changing the values of μ and it's corresponding the *LLE* are displayed in Figure 11.

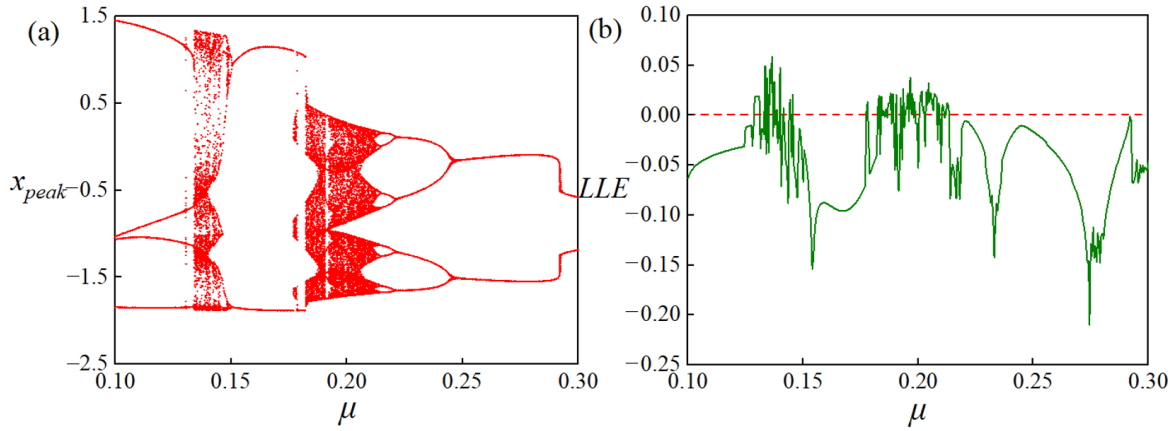


Figure 11. Firing behavior of neuron for varying μ. For (**a**) Evolution of bifurcation diagram; (**b**) *LLE* curve.

From Figure 11, as the parameter μ increases, the periodic firing behavior can be induced to exhibit chaotic electrical activity characteristics. When the parameter μ is further increased, the chaotic characteristics transform into periodic characteristics, and then return to chaotic characteristics again. Under the the continuous increase of parameter μ, the chaotic electrical activity characteristics eventually evolve into periodic discharge behavior. Furthermore, the firing sequences under values of μ are Figure 12.

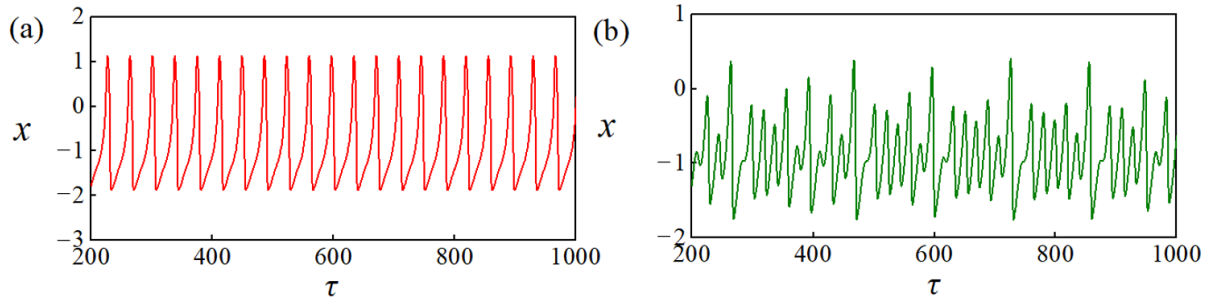


Figure 12. The firing sequences corresponding to value of μ. For (**a**) $\mu = 0.16$; (**b**) $\mu = 0.19$.

It can be clearly observed from Figure 12 that the periodic and chaotic firing behaviors induced by parameter a at different values. When parameters in Equation (6) are $a = 0.25$, $\beta = 0.8$, $\mu = 0.2$, initial value and the external periodic stimuli is kept as defined above, bifurcation diagram by changing the values of η and its corresponding the *LLE* are displayed in Figure 13.

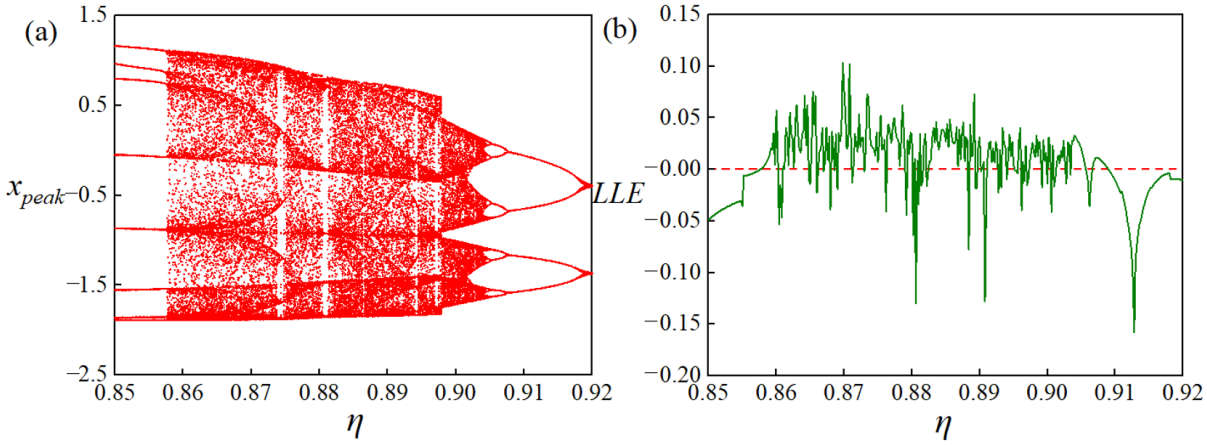


Figure 13. Firing behavior of neuron for varying η. For (**a**) Evolution of bifurcation diagram; (**b**) *LLE* curve.

Similarly, as the parameter η increases, the periodic firing behavior can be induced to exhibit chaotic electrical activity characteristics. With the continuous increase of parameter η, the chaotic electrical activity characteristics eventually evolve into periodic discharge behavior. Furthermore, the firing sequences under values of η are Figure 14.

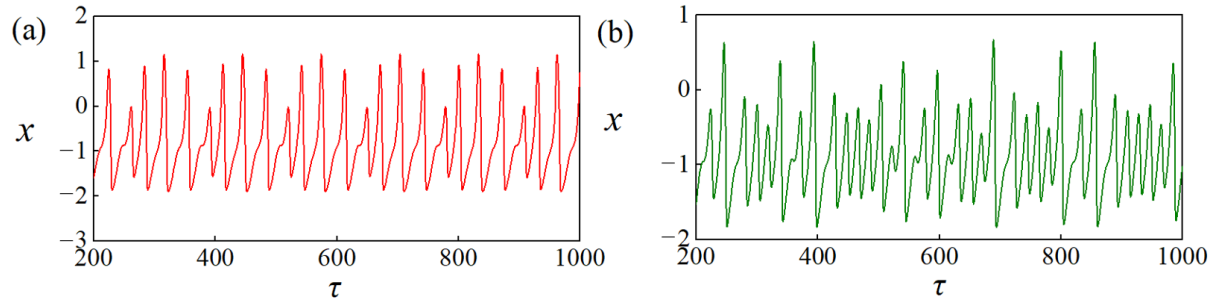


Figure 14. The firing sequences corresponding to value of η. For (**a**) $\eta = 0.8$; (**b**) $\eta = 0.89$.

Figure 14 shows that the chaotic firing behavior exhibits disorder and non-periodicity, while the periodic firing behavior has a high degree of orderliness. Furthermore, by using the SE complexity, this paper further explores the characteristics of neuronal electrical activity when two parameters simultaneously changed. The result is shown in Figure 15.

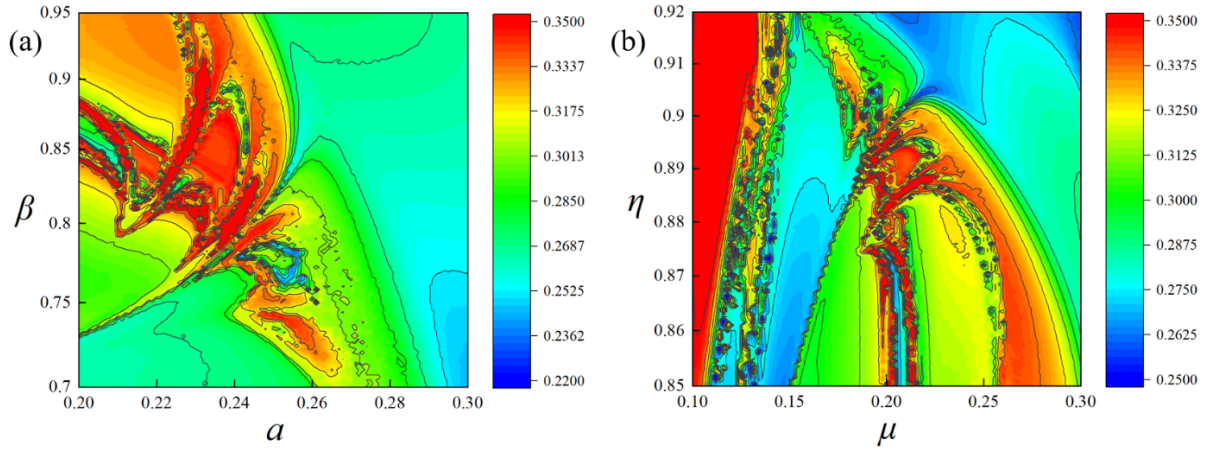


Figure 15. *SE* complexity. Initial value is (0.1, 0.1).

From Figure 15, the color scale represents relative SE complexity levels; red regions correspond to higher SE complexity values and do not by themselves indicate chaos.

Neurons are regarded as charged entities and are vulnerable to external magnetic fields. Therefore, investigating the impact of external magnetic fields on the electrical activities of neurons is an interesting research

topic. At first, parameters in Equation (7) are $a = 0.25$, $\beta = 0.8$, $\mu = 0.2$, $\eta = 0.9$, initial value is (0.1, 0.1), and the external periodic stimuli is $u_s = 0.055\cos(0.34\tau)$. for case of $S_{ext} = E$, bifurcation diagram by changing the values of E and its corresponding the *LLE* are displayed in Figure 16.

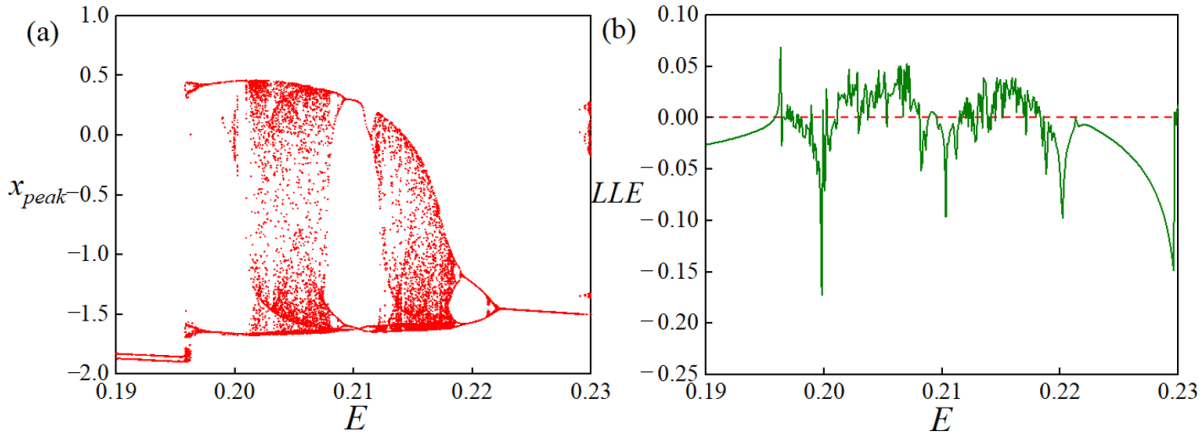


Figure 16. Firing behavior of neuron for varying E. For (**a**) Evolution of bifurcation diagram; (**b**) *LLE* curve.

From Figure 16, as the external magnetic field intensity E increases, the periodic electrical activity behavior evolves into chaotic electrical activity characteristics. As the intensity of E continues to increase, the chaotic behaviors can be suppressed, and periodic firing behavior occurs. Under the continuous increase of E, the periodic firing behavior evolves into chaotic behavior, and finally re-evolves into a periodic pattern. For case of $S_{ext} = B\cos(0.34\tau)$, when parameters and initial value are kept as above, the result is given in Figure 17.

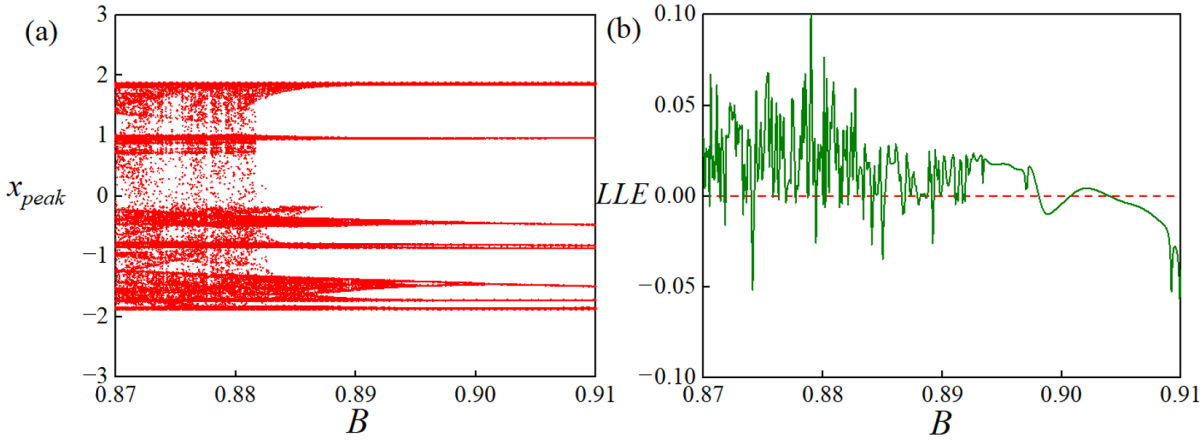


Figure 17. Firing behavior of neuron for varying B. For (**a**) Evolution of bifurcation diagram; (**b**) *LLE* curve.

Figure 17 shows that as the amplitude of the external periodic magnetic field increases, the chaotic electrical activity behavior evolves into a periodic electrical activity characteristic. In fact, a nonlinear model can occur the phenomenon of stochastic resonance when subjected to both periodic external stimulation and noise stimulation simultaneously. To investigate the phenomenon of stochastic resonance exhibited by the neurons described by the nonlinear equation proposed in this paper, a Gaussian white noise signal from the outside is selected. When *Eext* is considered as a Guassian white noise, and it is defined by

$$\langle \xi(\tau) \rangle = 0, \langle \xi(\tau)\xi(\tau') \rangle = 2D\delta(\tau - \tau'), \tag{8}$$

where $\langle * \rangle$ is the average, D denotes the noise intensity and $\delta(*)$ is Dirac-δ function. Parameters in Equation (7) are $a = 0.25$, $\beta = 0.8$, $\mu = 0.2$, $\eta = 0.9$, initial value is (0.1, 0.1), and the external periodic stimuli is $u_s = 0.055\cos(0.34\tau)$. Figure 18 shows the variation of SNR with external noise intensity D.

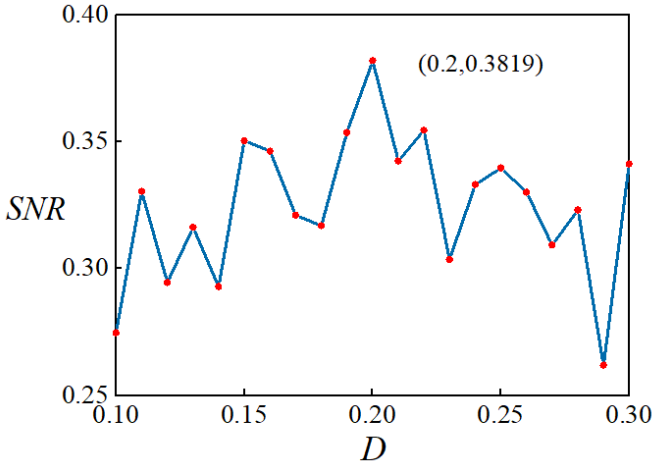


Figure 18. SNR for varying values of *D*.

From Figure 18, when $D = 0.2$, the SNR reaches a peak value of 0.389. This indicates that at this noise intensity, the neurons exhibited a phenomenon of stochastic resonance, and the membrane potential of the neurons became highly ordered. For verification of the analog circuit emulation, Equation (6) can be expressed equivalently as follows

$$\begin{cases} C_1 \dfrac{dV_1}{dt} = -\dfrac{R_5}{R_8 R_1} V_1 + \dfrac{R_5}{R_8 R_2} V_1^3 + \dfrac{R_5}{R_8 R_3}\left(\dfrac{R_{20}}{R_{22}} V_2 - \dfrac{R_{20}}{R_{21}} V_2^3\right) - \dfrac{R_5}{R_8 R_4} V_{S1} \\ C_2 \dfrac{dV_2}{dt} = -\dfrac{R_{13}}{R_{16} R_{11}} V_1 - \dfrac{R_{13}}{R_{16} R_{12}} V_{S2} \end{cases} \tag{9}$$

The equivalent circuit for Equation (9) is depicted in Figure 19.

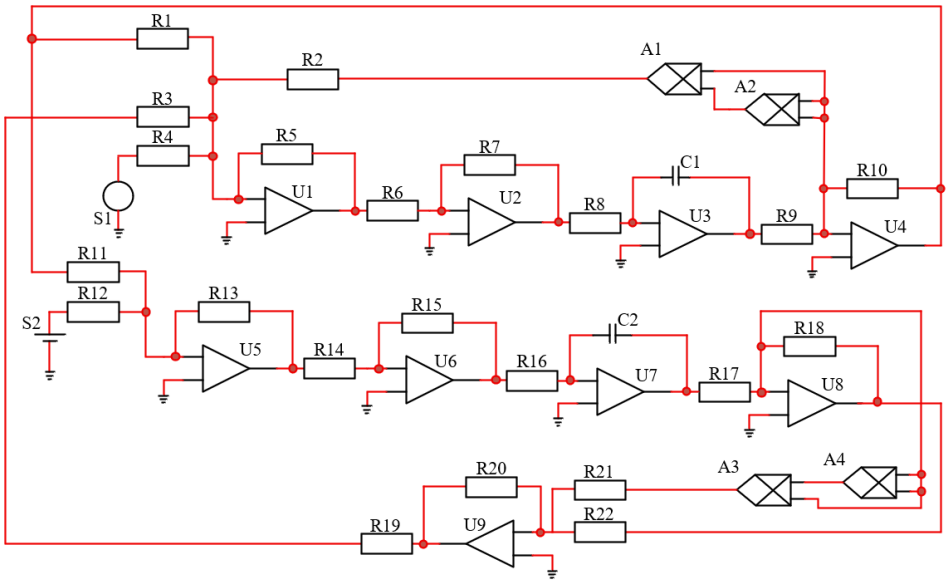


Figure 19. The equivalent circuit for Equation (9).

In Figure 19, the values of the electronic components are as follows

$$\begin{aligned} &R_i = 1M\Omega (i = 4,5,8,12,13,16,19,20,21), R_j = 100k\Omega (j = 6,7,9,10,14,15,17,18) \\ &R_1 = 1333.33k\Omega, R_2 = 3M\Omega, R_3 = 1176.47k\Omega, R_{11} = 5M\Omega, R_{22} = 6M\Omega, \end{aligned} \tag{10}$$

As a result, the LTspice simulation result is shown in Figure 20a. When parameters in Equation (6) are a = 0.25, β = 0.8, μ = 0.2, η = 0.9. Initial values in Equation (6) are given as (0.1, 0.1) and $u_s = 0.055\cos(0.34\tau)$. A phase diagram is Figure 20b.

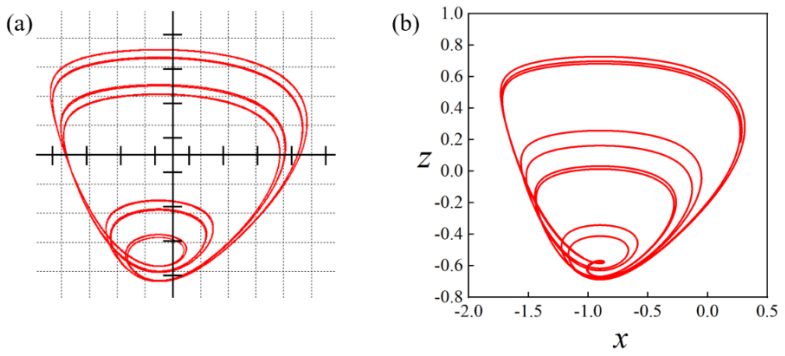


Figure 20. Phase diagrams. For (**a**) LTspice simulation result; (**b**) Numerical simulation result.

As shown in Figure 20, the results corroborate earlier numerical simulations, implying that the neuronal model is amenable to physical circuit implementation. Furthermore, neuron model is DSP (digital signal processor) realized. The hardware architecture block diagram of the neural system based on DSP is presented in Figure 21.

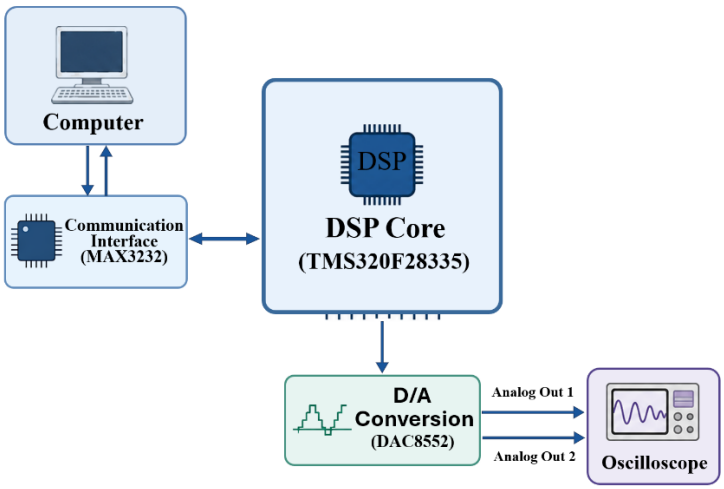


Figure 21. Hardware architecture block diagram based on DSP.

In Figure 21, the D/A converter uses the 16-bit channel DAC8552 chip, and the interface chip is MAX3232. In addition, a software flowchart for implementing neural systems based on DSP is displayed in Figure 22.

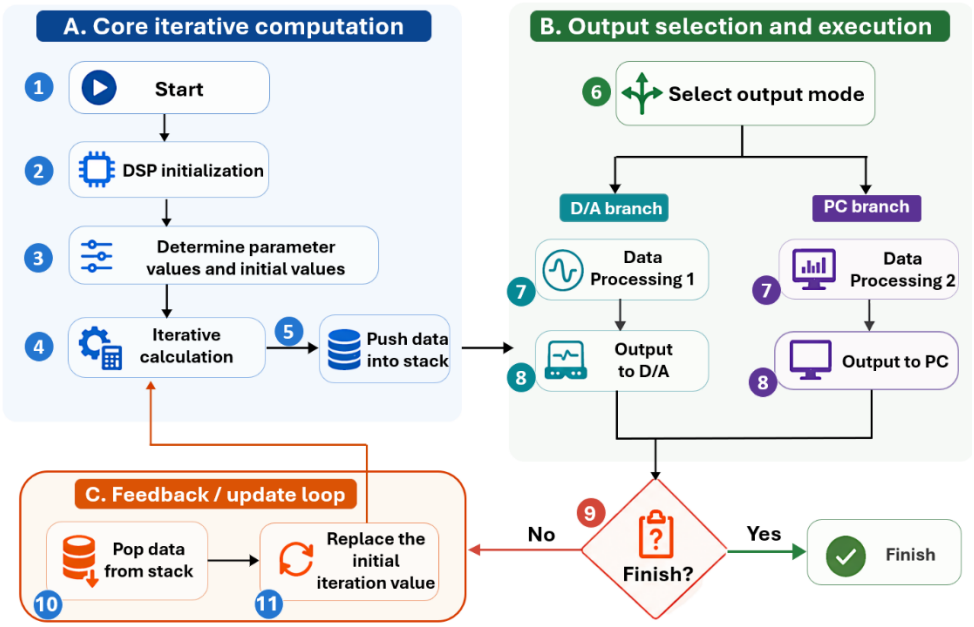


Figure 22. Software flowchart for implementing neural systems based on DSP.

Figure 23 is the experimental platform for implementing the neural system based on DSP.

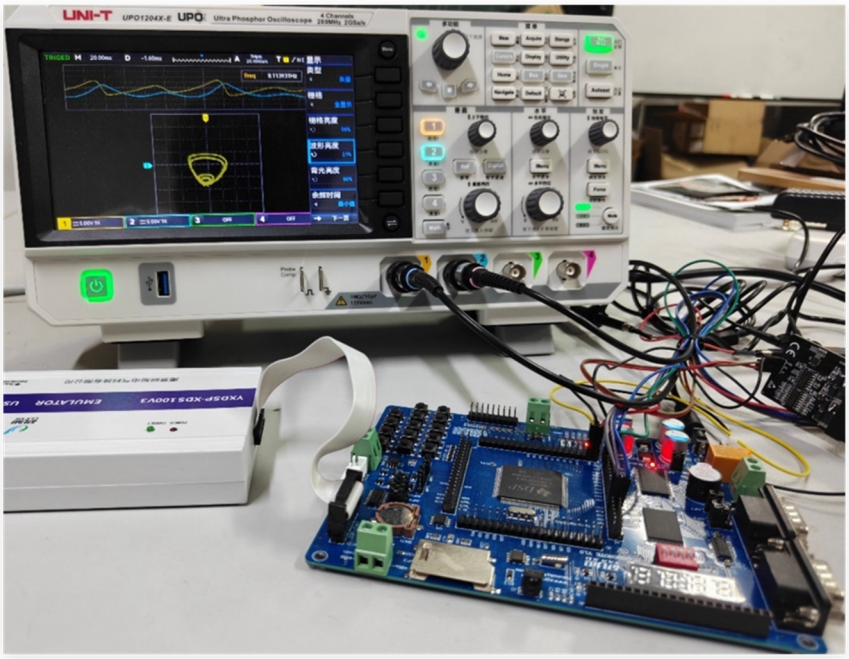


Figure 23. Experimental platform for implementing the neural system based on DSP.

The phase diagram displayed by the oscilloscope of the experimental platform is in agreement with the numerical simulation. This step indicates that the model can be realized in real time on the DSP platform. This will provide a theoretical basis for the practical application of the proposed neuron model.

To further compare the numerical and circuit-simulation results, the LTspice firing sequences under the same parameter conditions as those in Figure 3 are presented in Figure 24. For A = 0.055, the circuit simulation exhibits irregular firing, whereas a periodic firing sequence is obtained for A = 0.07. These results are consistent with the numerical firing sequences in Figure 3, supporting the circuit-level emulation of the modeled dynamics.

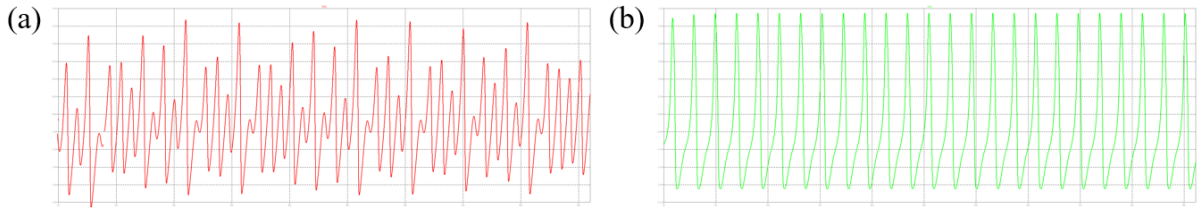


Figure 24. Comparison of LTspice circuit-simulation firing sequences under the parameter conditions of Figure 3. (**a**) A = 0.055; (**b**) A = 0.07.

4. Conclusions

This study constructed a circuit model of a *JJ* ion channel neuron and conducted a detailed analysis of the discharge patterns as well as the analog circuit emulation and DSP implementation. At first, a neural circuit is designed by a *JJ*, a capacitor, a nonlinear resistor and signal source. Kirchhoff's current laws are applied to obtain the circuit equations, which are then rescaled to yield a dimensionless multifunctional neuron model. The results showed that this model could reproduce selected periodic and chaotic firing-like dynamical patterns. Moreover, the model is verified through the analog circuit emulation and DSP implementation. The *JJ* ion channel neuron model established in this research has laid a solid theoretical and simulation foundation for the subsequent circuit realization of neuromorphic computing, brain-like perception, and adaptive control systems. In future work, we will consider constructing a physical *JJ* hardware platform to investigate the effects of junction geometry and magnetic flux on firing dynamics.

Author Contributions

K.Z.: Software and Data analysis. F.Y.: Methodology, Supervision, Writing—original draft and Writing—final version. All authors have read and agreed to the published version of the manuscript.

Funding

This research received no external funding.

Institutional Review Board Statement

Not applicable.

Informed Consent Statement

Not applicable.

Data Availability Statement

Data will be made available on request.

Conflicts of Interest

The authors declare no conflict of interest.

Use of AI and AI-Assisted Technologies

No AI tools were utilized for this paper.

References

1. Hodgkin, A.L.; Huxley, A.F. A quantitative description of membrane current and its application to conduction and excitation in nerve. *J. Physiol.* **1952**, *117*, 500–544. https://doi.org/10.1113/jphysiol.1952.sp004764.
2. FitzHugh, R. Impulses and Physiological States in Theoretical Models of Nerve Membrane. *Biophys. J.* **1961**, *1*, 445–466. https://doi.org/10.1016/s0006-3495(61)86902-6.
3. Nagumo, J.; Arimoto, S.; Yoshizawa, S. An Active Pulse Transmission Line Simulating Nerve Axon. *Proc. IRE* **1962**, *50*, 2061–2070. https://doi.org/10.1109/jrproc.1962.288235.
4. Morris, C.; Lecar, H. Voltage oscillations in the barnacle giant muscle fiber. *Biophys. J.* **1981**, *35*, 193–213. https://doi.org/10.1016/s0006-3495(81)84782-0.
5. Hindmarsh, J.L.; Rose, R.M. A model of the nerve impulse using two first-order differential equations. *Nature* **1982**, *296*, 162–164. https://doi.org/10.1038/296162a0.
6. Chay, T.R. Chaos in a three-variable model of an excitable cell. *Phys. D Nonlinear Phenom.* **1985**, *16*, 233–242. https://doi.org/10.1016/0167-2789(85)90060-0.
7. Izhikevich, E.M. Simple model of spiking neurons. *IEEE Trans. Neural Netw.* **2003**, *14*, 1569–1572. https://doi.org/10.1109/tnn.2003.820440.
8. Muni, S.S.; Fatoyinbo, H.O.; Ghosh, I. Dynamical Effects of Electromagnetic Flux on Chialvo Neuron Map: Nodal and Network Behaviors. *Int. J. Bifurc. Chaos* **2022**, *32*, 2230020. https://doi.org/10.1142/s0218127422300208.
9. Chen, X.; Wang, N.; Wang, K.; et al. Coupling dynamics in an FHN bi-neuron model coupled via ReLU function-based locally active memristor. *Nonlinear Dyn.* **2024**, *112*, 20365–20379. https://doi.org/10.1007/s11071-024-10127-7.
10. Nie, H.; Liu, J.; Shu, Y.; et al. Synchronization of the memristor-coupled memristive complex-valued FHN neurons. *Eur. Phys. J. Plus* **2025**, *140*, 918.
11. Tan, Y.; Wang, C. A simple locally active memristor and its application in HR neurons. *Chaos Interdiscip. J. Nonlinear Sci.* **2020**, *30*, 053118. https://doi.org/10.1063/1.5143071.
12. Zhang, S.; Zheng, J.; Wang, X.; et al. A novel no-equilibrium HR neuron model with hidden homogeneous extreme multistability. *Chaos Solitons Fractals* **2021**, *145*, 110761. https://doi.org/10.1016/j.chaos.2021.110761.
13. Bao, H.; Liu, W.; Ma, J.; et al. Memristor Initial-Offset Boosting in Memristive HR Neuron Model with Hidden Firing Patterns. *Int. J. Bifurc. Chaos* **2020**, *30*, 2030029. https://doi.org/10.1142/s0218127420300293.
14. Vivekanandhan, G.; Natiq, H.; Merrikhi, Y.; et al. Dynamical Analysis and Synchronization of a New Memristive Chialvo Neuron Model. *Electronics* **2023**, *12*, 545. https://doi.org/10.3390/electronics12030545.

15. Yu, X.; Huang, L.; Mou, J.; et al. Locally Active Memristor Cooperatively-Controlled Fast-Slow Dynamics in Morris–Lecar Neuron Model and FPGA Implementation. *IEEE Trans. Cybern.* **2026**, *56*, 1153–1164. https://doi.org/10.1109/tcyb.2025.3606973.
16. Liu, B.; Peng, X.; Li, C. Firing behaviors of memristor-based Rulkov neuron map using energy method. *AEU-Int. J. Electron. Commun.* **2024**, *178*, 155283. https://doi.org/10.1016/j.aeue.2024.155283.
17. Yu, Z.; Cui, H.; Song, X.; et al. Firing patterns of a multifunctional neural circuit with memristive membrane. *J. Supercomput.* **2025**, *81*, 1469. https://doi.org/10.1007/s11227-025-07980-7.
18. Yang, F.; Song, X.; Yu, Z. Dynamics of a functional neuron model with double membranes. *Chaos Solitons Fractals* **2024**, *188*, 115496. https://doi.org/10.1016/j.chaos.2024.115496.
19. Song, X.; Zhang, G.; Yang, F.; et al. Modeling and dynamics of a hybrid memristor-coupled neuron. *Nonlinear Dyn.* **2026**, *114*, 529.
20. Yu, Z.; Zhu, K.; Wang, Y.; et al. Dynamics of a neuron with a hybrid memristive ion channel. *Chaos Solitons Fractals* **2025**, *194*, 116233. https://doi.org/10.1016/j.chaos.2025.116233.
21. Yang, F.; Song, X.; Yu, Z. Adaptive mode selection of electrical activities in a neuron with a memristive ion channel. *Nonlinear Dyn.* **2025**, *113*, 7213–7222. https://doi.org/10.1007/s11071-024-10710-y.
22. Song, X.L.; Zhang, G.; Yang, F.F. A sound-sensitive neuron incorporating a memristive-ion channel. *Chin. Phys. B* **2025**, *34*, 120502. https://doi.org/10.1088/1674-1056/ae0563.
23. Yang, F.; Ma, J.; Ren, G. A Josephson junction-coupled neuron with double capacitive membranes. *J. Theor. Biol.* **2024**, *578*, 111686. https://doi.org/10.1016/j.jtbi.2023.111686.
24. Shao, Y.; Wu, F.; Wang, Q. Bursting dynamics and synchronization of neuromorphic systems with VO2 memristors and Josephson junctions. *Nonlinear Dyn.* **2025**, *113*, 33907–33926. https://doi.org/10.1007/s11071-025-11757-1.
25. Wang, B.; Ren, G.; Ma, J.; et al. A memristive neuron with double capacitive variables coupled by Josephson junction. *Chaos Solitons Fractals* **2025**, *198*, 116630. https://doi.org/10.1016/j.chaos.2025.116630.
26. Song, X.; Wang, Y.; Yang, F. A map neuron with a hybrid ion channel and its dynamics. *Commun. Theor. Phys.* **2025**, *77*, 085801. https://doi.org/10.1088/1572-9494/adb5f4.
27. Lei, Z.; Ma, J. Coherence resonance and energy dynamics in a memristive map neuron. *Chaos Interdiscip. J. Nonlinear Sci.* **2025**, *35*, 023158. https://doi.org/10.1063/5.0251352.
28. Guo, Q.; Ren, G.; Wang, C.; et al. Reliability and energy function of an oscillator and map neuron. *BioSystems* **2025**, *251*, 105443. https://doi.org/10.1016/j.biosystems.2025.105443.
29. Yang, F.; Ma, J.; Wu, F. Review on memristor application in neural circuit and network. *Chaos Solitons Fractals* **2024**, *187*, 115361. https://doi.org/10.1016/j.chaos.2024.115361.
30. Yang, F.; Song, X.; Zhang, G.; et al. Review on memristor application in discrete chaotic system and discrete neuron system. *Commun. Theor. Phys.* **2026**, *78*, 097801. https://doi.org/10.1088/1572-9494/ae7b16.
31. Li, X.; Guo, W.; Du, Y. Dynamical Analysis and Circuit Implementation of HR-FHN Neuron Model Coupled by Locally Active Memristor. *Int. J. Bifurc. Chaos* **2024**, *34*, 2430034. https://doi.org/10.1142/s0218127424300349.
32. Mou, J.; Cao, H.; Zhou, N.; et al. An FHN-HR Neuron Network Coupled With a Novel Locally Active Memristor and Its DSP Implementation. *IEEE Trans. Cybern.* **2024**, *54*, 7333–7342. https://doi.org/10.1109/tcyb.2024.3471644.
33. Ren, G.; Xu, Y.; Wang, C. Synchronization behavior of coupled neuron circuits composed of memristors. *Nonlinear Dyn.* **2017**, *88*, 893–901. https://doi.org/10.1007/s11071-016-3283-2.
34. Guo, Y.; Zhu, Z.; Wang, C.; et al. Coupling synchronization between photoelectric neurons by using memristive synapse. *Optik* **2020**, *218*, 164993. https://doi.org/10.1016/j.ijleo.2020.164993.
35. Xie, Y.; Wang, X.; Li, X.; et al. Energy consumption in the synchronization of neurons coupled by electrical or memristive synapse. *Chin. J. Phys.* **2024**, *90*, 64–82. https://doi.org/10.1016/j.cjph.2024.05.033.
36. Yang, F.; Ma, J. Creation of memristive synapse connection to neurons for keeping energy balance. *Pramana* **2023**, *97*, 55. https://doi.org/10.1007/s12043-023-02530-3.
37. Xie, Y.; Yao, Z.; Ma, J. Phase synchronization and energy balance between neurons. *Front. Inf. Technol. Electron. Eng.* **2022**, *23*, 1407–1420. https://doi.org/10.1631/fitee.2100563.
38. Xie, Y.; Yao, Z.; Ma, J. Formation of local heterogeneity under energy collection in neural networks. *Sci. China Technol. Sci.* **2023**, *66*, 439–455. https://doi.org/10.1007/s11431-022-2188-2.
39. Yang, F.; Wang, Y.; Ma, J. Creation of heterogeneity or defects in a memristive neural network under energy flow. *Commun. Nonlinear Sci. Numer. Simul.* **2023**, *119*, 107127. https://doi.org/10.1016/j.cnsns.2023.107127.
40. Yang, F.; Hu, X.; Ren, G.; et al. Synchronization and patterns in a memristive network in noisy electric field. *Eur. Phys. J. B* **2023**, *96*, 80.
41. Njitacke, Z.T.; Takembo, C.N.; Awrejcewicz, J.; et al. Hamilton energy, complex dynamical analysis and information patterns of a new memristive FitzHugh-Nagumo neural network. *Chaos Solitons Fractals* **2022**, *160*, 112211. https://doi.org/10.1016/j.chaos.2022.112211.

42. Wang, C.; Lv, M.; Alsaedi, A.; et al. Synchronization stability and pattern selection in a memristive neuronal network. *Chaos Interdiscip. J. Nonlinear Sci.* **2017**, *27*, 113108. https://doi.org/10.1063/1.5004234.
43. Pershin, Y.V.; Di Ventra, M. Experimental demonstration of associative memory with memristive neural networks. *Neural Netw.* **2010**, *23*, 881–886. https://doi.org/10.1016/j.neunet.2010.05.001.
44. Abdalla, O.; Baran, A.Y.; Korkmaz, N.; et al. Investigation of Synchronization Control of the Memristive/Resistive-Coupled Neural Network with Noise Effect. *Int. J. Bifurc. Chaos* **2024**, *34*, 2450099. https://doi.org/10.1142/s0218127424500998.
45. Bao, H.; Zhang, Y.; Liu, W.; et al. Memristor synapse-coupled memristive neuron network: Synchronization transition and occurrence of chimera. *Nonlinear Dyn.* **2020**, *100*, 937–950. https://doi.org/10.1007/s11071-020-05529-2.
46. Yang, S.; Guo, Z.; Wang, J. Robust Synchronization of Multiple Memristive Neural Networks With Uncertain Parameters via Nonlinear Coupling. *IEEE Trans. Syst. Man Cybern. Syst.* **2015**, *45*, 1077–1086. https://doi.org/10.1109/tsmc.2014.2388199.
47. Yang, X.; Ho, D.W.C. Synchronization of Delayed Memristive Neural Networks: Robust Analysis Approach. *IEEE Trans. Cybern.* **2015**, *46*, 3377–3387. https://doi.org/10.1109/tcyb.2015.2505903.
48. Ma, J. Biophysical neurons, energy, and synapse controllability: A review. *J. Zhejiang Univ.-Sci. A* **2023**, *24*, 109–129. https://doi.org/10.1631/jzus.a2200469.
49. Ma, J.; Tang, J. A review for dynamics in neuron and neuronal network. *Nonlinear Dyn.* **2017**, *89*, 1569–1578. https://doi.org/10.1007/s11071-017-3565-3.
50. Lin, H.; Wang, C.; Deng, Q.; et al. Review on chaotic dynamics of memristive neuron and neural network. *Nonlinear Dyn.* **2021**, *106*, 959–973. https://doi.org/10.1007/s11071-021-06853-x.
51. Baysal, V.; Çakırgöz, O.; Jafari, S.; et al. A computational modeling study of the effects of background chaotic spike trains on the signal processing of Hodgkin–Huxley neuron. *Chaos Solitons Fractals* **2026**, *205*, 117816. https://doi.org/10.1016/j.chaos.2025.117816.